ORIGINAL ARTICLE

Rock slope stability charts based on limit equilibrium method incorporating Generalized Hoek–Brown strength criterion for static and seismic conditions

Vinay Kumar[1] · Avijit Burman[1] · Navneet Himanshu[2] · Behrouz Gordan[3]

Abstract
Stability charts present a graphical approach for the estimation of factor of safety (FOS) of a finite slope with uniform soil properties which are routinely used by geotechnical engineers. They provide a way for quick and efficient determination of stability of slopes sidestepping the need for carrying out actual analysis. In the present work, authors have developed stability charts of rock mass to determine global minimum FOS for rock slope stability problems. The rock mass is modelled by incorporating generalized Hoek–Brown strength criterion proposed by Hoek et al. (Hoek–Brown criterion—2002 edition, 2002). Limit equilibrium technique based Morgenstern and Price (Géotechnique 15:79–93, 1965) method is used to determine the value of factor of safety of the rock slope against failure. An evolutionary optimization method i.e. Particle swarm optimization (PSO) is used to search for the minimum FOS values and the associated critical failure surface out of all possible slip surfaces. A MATLAB code has been developed for this purpose. The charts have been developed for the entire range of Geological Strength Index (GSI) values ranging from 0 to 100 for intact rock mass characterized by the disturbance factor $D = 0$ for both static and seismic loading conditions. The seismic slope analysis is performed by an equivalent static method using a horizontal seismic coefficient (k_h) with values ranging from 0.10 to 0.30. Stability charts contain stability numbers which are inversely proportional to FOS value of the slope. In the present work, stability numbers are plotted for different inclination angles (β) equal to 15°, 30°,45°, 60° and 75$^{+°}$, respectively, for both static and seismic conditions considering the variations of other material parameters such as m_i and GSI. Stability numbers are observed to increase with an increase in angle of inclination (β) of the slope and correspondingly FOS values follow a decreasing trend. However, stability numbers follow a decreasing pattern with increasing values of material parameters m_i and GSI designating improved rock quality with corresponding increase in FOS values of the rock slope.

✉ Avijit Burman
avijitburman@yahoo.com; avijit@nitp.ac.in

Vinay Kumar
vinay1.ce16@nitp.ac.in

Navneet Himanshu
navneet.ce2020@niet.co.in

Behrouz Gordan
bh.gordan@yahoo.com

1 Department of Civil Engineering, Geotechnical Engineering, NIT Patna, Bihar, India

2 Department of Civil Engineering, Noida Institute of Engineering and Technology, Greater Noida, Uttar Pradesh, India

3 Civil Engineering Department, Islamic Azad University, Hamedan Branch, Hamadan, Iran

Introduction

In previous decades, different strength criteria were suggested by various researchers to calculate the shear strength of the rock mass based on Hoek–Brown strength criterion (Hoek 1983; Londe 1988; Hoek and Brown 1997; Kumar 1998; Hoek et al. 2002; Carranza-Torres 2004; Priest 2005; Shen et al. 2012b, a). The nonlinear generalized Hoek–Brown failure criterion (Hoek et al. 2002) is famous among the scientist for determining the strength of rock mass. This criterion became widely popular among the researchers for estimating the shear strength of various types of intact and fractured rock mass (Priest 2005). Amongst other popular strength criterion for expressing soil/rock mass behavior such as Mohr–Coulomb criterion,

more than one input parameters i.e. cohesion, angle of internal friction, dilation angles are needed. On the other hand, Hoek–Brown criterion uses uniaxial compressive strength (σ_{ci}), m_i and GSI as input parameters. Also, the initial condition and damage state of the material can be simulated in the criterion. When rock samples are tested in triaxial set up, their normal stress vs shear stress behavior shows a nonlinear pattern (Hoek 1983). Mohr–Coulomb failure criteria states that the relationship between normal and shear stress is linear. Hoek–Brown (1983) failure criteria and Generalized Hoek–Brown failure criteria (Hoek et al. 2002) are able to represent the nonlinear nature of the normal stress vs shear stress pattern of rock material. Because of nonlinear nature of normal stress vs shear stress behavior, it is necessary to determine instantaneous cohesion and instantaneous angle of internal friction while dealing with rocks. For linear Mohr–Coulomb criteria, cohesion and angle of internal friction will always remain constant over the entire range of failure envelop. Therefore, if Mohr–Coulomb failure criteria is used for representing rock material, the nonlinear normal stress vs shear stress pattern will not be properly modelled. The changing nature of both cohesion and angle of internal friction can be better evaluated from Hoek–Brown (1983) and generalized Hoek–Brown (Hoek et al. 2002) yield criteria over the entire range of failure envelop. Also, Mohr–Coulomb failure criteria gives a larger value of tensile strength compared to the tensile strength predicted by Hoek–Brown criteria (1983). Triaxial test results reveal that the tensile strength of rock predicted by Hoek–Brown criteria is nearer to the actual values. Furthermore, generalized Hoek–Brown (Hoek et al. 2002) introduced a disturbance factor D which could be used to represent the initial damage state of the rock material in a very simple manner by considering the values of disturbance factor ranging from 0 to 1. This ability of considering initial damage state of the material is not available with Mohr–Coulomb failure criteria. Shi et al. (2016) developed modified form of Hoek–Brown failure criterion for anisotropic rock mass. Such flexibility obviously puts Hoek–Brown criterion in an advantageous position for expressing properties of rock materials. Ismael et al. (2014) suggested a simplified approach to directly consider intact rock anisotropy in Hoek–Brown failure criterion. Zuo et al. (2015) developed a different approach for theoretical derivation of the Hoek–Brown failure criterion for rock materials. In recent time, Hoek and Brown (2019) have demonstrated the practical application of the failure criterion using the parameter Geological Strength Index (GSI).

Recently, many researchers have performed the stability analysis of rock mass based on Hoek–Brown strength criterion. In geotechnical engineering, the stability analysis of the rock slope is an important problem and plays a major role when designs of tunnel, dam, road and other civil engineering structure are carried out. Sari (2019) analyzed the stability of cut slopes using empirical, kinematical, numerical and limit equilibrium methods. The problem of rock slope stability is a challenging task and engineers have concentrated on assessing the slope stability of rock mass (Hoek and Bray 1981; Goodman 1989; Wyllie and Mah 2004; Basahel and Mitri 2017). Analysis of rock slopes requires evaluation of factor of safety (FOS) for the sliding mass. Limit equilibrium techniques (Fellenius 1936; Janbu 1954; Bishop 1955; Lowe and Karafiath 1960; Morgenstern and Price 1965; Spencer 1967) are most famous among researchers for determination of FOS of any slopes against failure. In this context, stability charts have become a convenient way of determining the stability of any slope problem without carrying out extensive calculations. Taylor (1937) had developed first stability charts for soil slope based on limit equilibrium technique. Afterwards, many investigators have tried to develop stability chart for rock slope based on rock mass strength criteria, but it has proven very demanding task due to the difficulty involved in assessing the strength of rock mass. Many researchers have given idea to overcome the problem of estimating rock slope strength and analysis of rock slope stability such (Jaeger, 1971; Goodman and Kieffer 2000). For rock masses, the stability charts developed by Hoek and Bray (1981) serve the purpose of quick estimation of factor of safety of rock slopes for different slope geometries. Zanbak (1983) had developed stability charts for rock slopes susceptible to toppling. Lyamin and Sloan (2002) and Krabbenhoft et al. (2005) have developed finite element upper and lower bound technique for true stability solutions for geotechnical problem. Furthermore, stability charts were presented by Siad (2003) based on the upper bound approach which is useful for estimating FOS of rock slopes under seismic excitations.

Later, Li et al. (2008) developed stability chart-based solution based on Hoek–Brown criteria using numerical limit analysis. Li et al. (2009) also suggested stability chart solution based on limit analysis methods considering seismic effects on rock mass. In their work, pseudo-static method for determining the rock slope stability was adopted. More recently, Belghali et al. (2017) performed the pseudo-static stability analysis of rock slopes reinforced by passive bolts using the generalized Hoek–Brown criterion. Sun et al. (2019) performed experimental and numerical investigations of the seismic response of a rock–soil mixture deposit slope.

Furthermore, most of the earlier works on rock slope stability charts were based on limit analysis methods (Lyamin and Sloan 2002; Krabbenhoft et al. 2005; Li et al. 2008, 2009). It is a well-known fact that the upper bound limit analysis of slope will overestimate the factor of safety (FOS) of the slope; whereas, the lower bound limit analysis usually underestimates the FOS value unless the solutions are not exact. True or exact value of FOS will only be obtained if both upper and lower bound analysis show true convergence

(Huang et al. 2013). That is why, traditional limit equilibrium approach with an appropriate optimization algorithm to find out the lowest FOS value and associated critical failure surface is deemed more reliable. Little efforts have been made to develop rock slope stability charts based on limit equilibrium techniques involving a proper optimization approach to arrive at the minimum FOS value and the corresponding critical failure surface incorporating GHB strength criteria. It is further observed that limit equilibrium-based approaches of rock slope analyses had used the concept of circular failure surfaces during slope analysis (Deng et al. 2017). The consideration of circular shape of failure surface may not represent the actual shape of failure surface. In this regard, a failure surface composed of piecewise linear segments is deemed more suitable for representing the actual shape failure surface as it has the ability to represent any general shape of failure surface. Recently, Kumar et al. (2019a, b) carried out rock slope analysis based on limit equilibrium method where failure surface was assumed to be composed of piecewise linear segments.

In this paper, authors have developed stability charts of rock mass to determine the global minimum FOS for rock slope stability problems. An appropriate nonlinear strength criterion is used in the form of generalized Hoek–Brown (GHB) criteria proposed by Hoek et al. (2002). Limit Equilibrium technique based Morgenstern and Price (1965) method is utilized to determine the value of factor of safety of the rock slope against failure. The method was developed specifically for any general shape of failure surface, including circular as well as non-circular shape, and it satisfies both force and moment equilibrium of all slices inside the failure mass. In the present work, trial failure surfaces are generated using piecewise linear segments which is considered suitable for representing any general shape of the failure surface. An evolutionary optimization method i.e. Particle Swarm Optimization (PSO) is used to search for the minimum FOS values and the associated critical failure surface out of all possible slip surfaces (Kumar et al. 2019a; Himanshu et al. 2020). Stability charts have been developed for both static and seismic loading conditions of intact rock slopes with different angle of inclinations (β) = 15°, 30°, 45°, 60° and 75°. A MATLAB code has been developed for this purpose. The charts have been developed for entire range of Geological Strength Index (GSI) values ranging from 0 to 100 for intact rock mass characterized by the disturbance factor $D = 0$. Both static and seismic analyses have been carried out while developing the stability charts for intact rock mass. Different values of horizontal seismic coefficients have been used while developing the charts considering seismic loading.

Methodology and modelling

Generalized Hoek–Brown failure criterion

To model the failure characteristics of different types intact and fractured rock mass, Hoek and Brown (1980, 1997) proposed the nonlinear failure criterion which gained popularity amongst researchers all over the world. Recently, a Generalized Hoek–Brown failure criterion (GHB) was proposed by Hoek et al. (2002) after modifying the originally proposed yield criterion. The GHB criterion is expressed as follows:

$$\sigma_1 = \sigma_3 + \sigma_{ci}\left\{\left(\frac{m_b\sigma_3}{\sigma_{ci}}\right) + s\right\}^a, \tag{1}$$

where σ_1 = major effective principal stress at failure.

σ_3 = minor effective principal stress at failure.

σ_{ci} = uniaxial compressive strength of the intact rock material.

Here, s, m_b and a are Hoek–Brown material parameters. The parameter m_b depends on its initial value m_i. The parameters s and a depend on the characteristics of the rock mass. These parameters are further expressed as functions of Geological Strength Index (GSI) of the rock mass and a disturbance D. The GSI values usually range from 0 to 100. A GSI value of 0 represents a rock mass of very poor quality; whereas, a value equal to 100 signifies intact rock with very good strength. The degree of interlocking of constituent blocks inside any rock mass is expressed using the term GSI. Hoek et al.(2002) introduced a disturbance factor D to express the presence of initial disturbance in the rock mass caused by stress relaxation and damage. The expressions of s, m_b and a are as follows:

$$m_b = m_i \exp\left(\frac{GSI - 100}{28 - 14D}\right), \tag{2}$$

$$s = \exp\left(\frac{GSI - 100}{9 - 3D}\right), \tag{3}$$

$$a = 0.5 + \frac{e^{\left(\frac{-GSI}{15}\right)} - e^{\left(\frac{-20}{3}\right)}}{6}, \tag{4}$$

where, m_i is the Hoek–Brown constant for intact rock. Thus, Eqs. (3)–(4) cover the whole range of GSI values (0–100) in a very effective way. The generalized expression of the Hoek–Brown failure criterion in Eq. (1) can be represented as follows:

$$\sigma_1 = \sigma_3 + \sigma_{ci}\left(m_f\right)^a, \tag{5}$$

where

$$m_{\mathrm{f}} = \left(\frac{m_b \sigma_3}{\sigma_{\mathrm{ci}}} \right) + s. \tag{6}$$

In the Hoek and Brown (1997) failure criterion, the parameter s was considered equal to zero for GSI less than 25. In GHB criterion proposed by Hoek et al.(2002), the parameter s is modified to assume a very low positive value for low values of GSI. The GHB criterion with non-zero s is adopted in the present work to model the rock mass.

Equation (5) expresses the relationship between major and minor principal stresses of any rock mass as per GHB criterion (Hoek et al. 2002). A relationship proposed by Balmer (1952) may be utilized to express Eq. (5) in terms of normal and shear stresses. The procedure is as follows:

$$\tau = \left(\sigma_n - \sigma_3 \right) \sqrt{\frac{\partial \sigma_1}{\partial \sigma_3}}, \tag{7}$$

$$\sigma_n = \sigma_3 + \frac{\sigma_1 - \sigma_3}{\frac{\partial \sigma_1}{\partial \sigma_3} + 1}. \tag{8}$$

Differentiating Eq. (1) with the respect of σ_3, we get

$$\frac{\partial \sigma_1}{\partial \sigma_3} = 1 + am_b \left(\frac{m_b \sigma_3}{\sigma_{ci}} + s \right)^{a-1}. \tag{9}$$

After substituting Eq. (9) into Eqs. (7) and (8), respectively, the GHB criterion can be modified as follows:

$$\tau = \left(\sigma_n - \sigma_3 \right) \sqrt{1 + am_b \left(\frac{m_b}{\sigma_{ci}} \sigma_3 + s \right)^{a-1}}, \tag{10}$$

$$\sigma_n = \sigma_3 + \frac{\sigma_{\mathrm{ci}} \left(\frac{m_b \sigma_3}{\sigma_{ci}} + s \right)^a}{2 + am_b \left(\frac{m_b \sigma_3}{\sigma_{ci}} + s \right)^{a-1}}. \tag{11}$$

From the nonlinear shear stress (τ) vs. normal stress $\left(\sigma_n \right)$ failure envelop, the instantaneous angle of internal friction φ_i can be expressed using general formula suggested by Balmer (1952):

$$\tan \phi_i = \frac{\partial \tau}{\partial \sigma_n}. \tag{12}$$

Finally, to calculate an instantaneous angle of internal friction φ_i, the following expression can be used (Shen et al. 2012a):

$$\varphi_i = \arcsin \left(1 - \frac{2}{2 + am_b \left(\frac{\sigma_3}{\sigma_{ci}} m_b + s \right)^{a-1}} \right). \tag{13}$$

The instantaneous cohesion can be calculated by solving the Mohr–Coulomb strength equation:

$$c_i = \tau - \sigma_n \tan \phi_i. \tag{14}$$

The instantaneous Mohr–Coulomb strength parameters (i.e. c_i and ϕ_i) are determined using Eqs. (7)–(14). Solving Eq. (11) is a challenging task since it is a nonlinear expression involving the term σ_3 which itself is initially unknown.

Solution of 2D Hoek–Brown yield criterion

Numerous triaxial tests on intact rocks of different types have revealed that the normal stress vs. shear stress behaviur is nonlinear (Hoek 1983). Therefore, it would be inappropriate to consider constant values of cohesion and angle of internal friction along the range of failure envelop as is done in case of linear Mohr–Coulomb failure criteria. Hoek (1983) stated that it would be more logical to estimate instantaneous effective cohesion $\left(c' \right)$ and instantaneous effective angle of internal friction $\left(\phi' \right)$ for rock materials under any applied normal stress $\left(\sigma_n \right)$. Equation (11) shows the GHB criteria as a function of normal stress $\left(\sigma_n \right)$, minor principal stress $\left(\sigma_3 \right)$ and known GHB material parameters s, m_b and a. While solving the generalized Hoek–Brown (GHB) strength criterion, the minor principal stress $\left(\sigma_3 \right)$ is determined from Eq. (11) for any known value of applied normal stress $\left(\sigma_n \right)$. After obtaining the value of minor principal stress $\left(\sigma_3 \right)$, Eqs. (13) and (14) are used to calculate the instantaneous values of Mohr–Coulomb shear strength parameters (i.e. φ_i and c_i). Many researchers (Kumar 1998; Priest 2005; Shen et al. 2012a, b) proposed their own expressions to obtain the value of minor principal stress $\left(\sigma_3 \right)$ from Eq. (11) and subsequently calculate the instantaneous Mohr–Coulomb shear strength parameters (i.e. φ_i and c_i). Recently, Kumar et al. (2019b) developed a numerical procedure using Newton–Raphson method to solve Eq. (11) for minor principal stress $\left(\sigma_3 \right)$ which is used in the present work for slope analysis and development of stability charts.

Generation of trial failure surface

Slope analysis using limit equilibrium technique starts with an assumption of any failure surface with a predetermined shape. It may be circular, logarithmic spiral or any other general shape. Different methods of trial failure surface generation and their performances have been reported earlier. Various researchers (Malkawi et al. 2001; McCombie and Wilkinson 2002; Cheng et al. 2007a, b; Kumar et al. 2019a) have discussed about different methods of generating trial failure surface and their performance in slope analysis. The trial failure surface must satisfy the condition of kinematic admissibility and should be concave upward.

These requirements are fulfilled by satisfying the following equation:

$$\alpha_1 < \alpha_2 < \cdots < \alpha_{nsls-1} < \alpha_{nsls}, \tag{15}$$

where α_i = angle of inclination of the base of the ith slice.

A simple technique for generating failure surface composed of piecewise linear segments is discussed in detail by Kumar et al. (2019a) and Himanshu et al. (2019). This method is used in the current work. The non-circular failure surface with discrete number of slices is characterized by three control variables $(x_1, x_r, \alpha_1, \alpha_r)$. The variables (x_1, y_1) and (x_r, y_r) describe the coordinates of initial and final intersection points of the slip surface with the ground surface. The angles α_1 and α_r represent the vertical inclination angles of the base of initial and final slices, respectively. The procedure is depicted in Fig. 1 for any general slope and a trial failure surface composed of piecewise linear segments. The ordinates of two end points y_1 and y_r are actually obtained using the equation of top surface of the slope $y_1^{surf}(x)$ for known values of (x_1, x_r) and therefore are treated as dependent variables. That is why, $(x_1, x_r, \alpha_1, \alpha_r)$ are treated as the controlling variable while generating the trial failure surface. Readers are requested to refer to the works of Kumar et al. (2019a) and Himanshu et al. (2019) where more details of the generation process of the non-circular trial failure surface can be found.

The objective function of PSO

Analysis of any slope, as per limit equilibrium method, depends on the mobilized downward force aiding the movement and the resisting shear force acting against it. The factor of safety (FOS) is defined as the ratio of the resisting force and the mobilizing force

$$f = \text{FOS} = \frac{\sum \text{Sr}_i}{\sum \text{Sm}_i}. \tag{16}$$

Here, $\sum \text{Sr}_i$ is the summation of the shear resistance and $\sum \text{Sm}_i$ is the summation of the mobilized shear. Zhu et al. (2005) presented an algorithm implementing Morgenstern and Price (1965) method for calculating FOS of any slope. A Matlab code was developed by Kumar et al. (2019a) implementing the algorithm presented by Zhu et al. (2005). In the present work, same code has been used for calculating the FOS of the rock slope implementing Morgenstern and Price (1965) method. A brief description of the algorithm is presented below:

Shear strength (resistance) of slice: $\text{Sr}_i = c'_i l_i + N'_i \tan \varphi'_i,$
$$\tag{17}$$

Shear stress (mobilized) ofslice: $\text{Sm}_i = (c'_i l_i + N'_i \tan \varphi'_i)/F.$
$$\tag{18}$$

Here, c'_i and ϕ'_i are effective cohesion and effective angle of internal friction applicable for the ith slice. Also, l_i and N'_i are the length of the base of the ith slice and the effective normal force on it, respectively. Also, F is the factor of safety applied to obtain developed or mobilized shear strength.

Morgenstern and Price (1965) method considers both inter-slice normal force (En) and inter-slice shear force (Es = $f^n \lambda$ En) with variable force function f^n along the slice as shown in Fig. 2. Here, λ is defined as scaling factor. In the present work, author uses a half-sine force function for f^n while evaluating FOS.
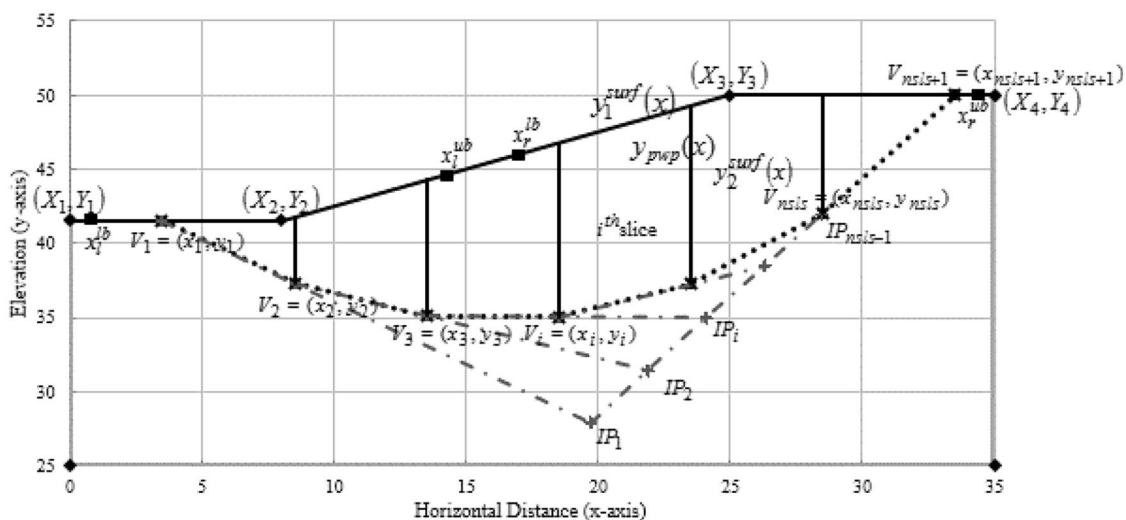

Fig. 1 Trial non-circular failure surface. (Source: Kumar et al. 2019a)
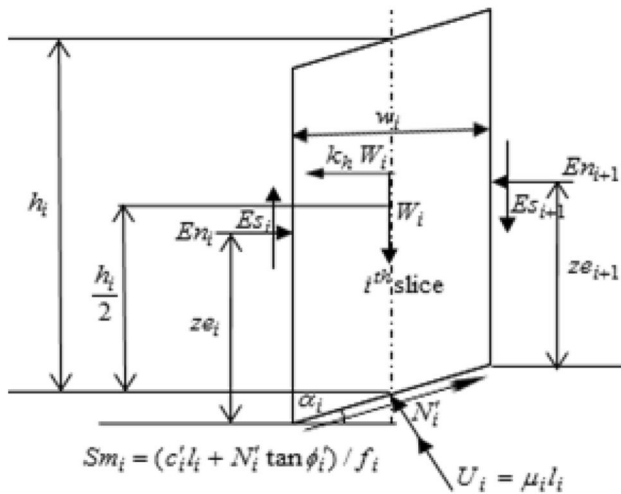
Fig. 2 Forces acting on ith slice

Figure 2 shows a typical slice (i) having width w_i, height h_i and base angle α_i. The base–normal N_i' is obtained by observing the equilibrium of all vertical forces acting on the slice as follows:

$$N_i' = (W_i + Es_{i+1} - Es_i)\cos\alpha_i + (-k_h W_i - En_{i+1} + En_i)\sin\alpha_i - U_i. \tag{19}$$

In Eq. (19), W_i, U_i and k_h are the weight, pore pressure and horizontal seismic coefficient for the ith slice. From the consideration of equilibrium of all horizontal forces on ith slice, the expression of mobilized shear force Sm_i can be obtained as follows:

$$Sm_i = (c_i' l_i + N_i' \tan\varphi_i')/F_i = (W_i + Es_{i+1} - Es_i) \\ \sin\alpha_i - (-k_h W_i - En_{i+1} + En_i)\cos\alpha_i. \tag{20}$$

Using the relationship $Es = f^n \lambda En$ and substituting Eq. (19) into Eq. (20), following expression can be obtained:

$$En_{i+1}[(\sin\alpha_i - f_{i+1}^n \lambda\cos\alpha_i)\tan\varphi_i' + (\cos\alpha_i + f_{i+1}^n \lambda\sin\alpha_i)F] - Sr_i' \\ = En_i[(\sin\alpha_i - f_i^n \lambda\cos\alpha_i)\tan\varphi_i' + (\cos\alpha_i + f_i^n \lambda\sin\alpha_i)F] - Sm_i'. \tag{21}$$

The forces Sr_i' and Sm_i' represent the total shear resistance and mobilized shear for any particular ith slice. The expressions of Sr_i' and Sm_i' are as follows:

$$Sr_i' = (W_i \cos\alpha_i - k_h W_i \sin\alpha_i - U_i)\tan\varphi_i' + c_i' l_i, \tag{22}$$

$$Sm_i' = W_i \sin\alpha_i + k_h W_i \cos\alpha_i. \tag{23}$$

Equation (21) is rearranged in a modified form as follows:

$$En_{i+1}\, \chi_{i+1}\, \eta_{i+1} = En_i\, \chi_i - F\, Sm_i' + Sr_i', \tag{24a}$$

$$\chi_i = (\sin\alpha_i - f_i^n \lambda\cos\alpha_i)\tan\varphi_i' + (\cos\alpha_i + f_i^n \lambda\sin\alpha_i)F, \tag{24b}$$

$$\chi_{i+1} = (\sin\alpha_{i+1} - f_{i+1}^n \lambda\cos\alpha_{i+1})\tan\varphi_{i+1}' + (\cos\alpha_{i+1} + f_{i+1}^n \lambda\sin\alpha_{i+1})F, \tag{24c}$$

$$\eta_{i+1} = [(\sin\alpha_i - f_{i+1}^n \lambda\cos\alpha_i)\tan\varphi_i' + (\cos\alpha_i + f_{i+1}^n \lambda\sin\alpha_i)F]\big/\chi_{i+1}. \tag{24d}$$

In Eq. (24a), the inter-slice normal forces should meet the boundary conditions i.e. boundary values for two end slices at left and right of the failure surface. The boundary values are: $En_1 = En_{nsls+1} = 0$. Using the conditions of force equilibrium, the factor of safety (FOS) can be obtained as:

$$FOS = F = \frac{Sr_1' + \sum_{i=2}^{i=nsls}\left(Sr_i' \prod_{j=2}^{j=i} \eta_j\right)}{Sm_1' + \sum_{i=2}^{i=nsls}\left(Sm_i' \prod_{j=2}^{j=i} \eta_j\right)}. \tag{25}$$

The readers are requested to refer to the work of Zhu et al. (2005) for more detailed description for solving Eq. (25).

Particle Swarm Optimization method to search for the critical failure surface

It is important to find out the critical failure surface with minimum FOS out of all possible failure surfaces. For this purpose, Particle Swarm Optimization (PSO) is used in the present work. While generating a segmented piecewise linear failure surface in the present work, four control variables are involved. The left most coordinate (x_l) and rightmost x-coordinate (x_r) of the trial failure surface constitute first two variables/particles. The angles made by the leftmost slice (α_l) and the rightmost slice (α_r) with the horizontal form the next two variables/particles. Any particle in the swarm is defined as:

$$P_i = (x_{il}, x_{ir}, \alpha_{il}, \alpha_{ir})^T \in A;\ i = 1, 2, 3, 4, \ldots, N. \tag{26}$$

The position (X_i^k) and velocity (V_i^k) are constantly updated as the particles move inside the search space A. Here k represents the number of iteration steps in PSO algorithm. Therefore,

$$X_i^k = \left(x_{i1}^k, x_{i2}^k, x_{i3}^k, x_{i4}^k\right) \in A,\ i = 1, 2, 3, 4, \ldots, N, \tag{27}$$

$$V_i^k = (v_{i1}^k, v_{i2}^k, v_{i3}^k, v_{i4}^k)^T \quad i = 1, 2, 3, 4, \ldots, N. \tag{28}$$

In the early form of PSO, each particle employs Eq. (29) to update their velocity (Eberhart and Kennedy 1995; Kennedy and Eberhart 1995; Eberhart et al. 1996)

$$V_i^{k+1} = V_i^k + c_1 \times \text{rand}_1 \times (X_{\text{pbest}}^k - X_i^k)$$
$$+ c_2 \times \text{rand}_2 \times (X_{\text{sbest}}^k - X_i^k). \qquad (29)$$

The early PSO variants (Shi and Eberhart 2008) are plagued by the problem of premature convergence and thus were unable to find the optimized solution. To alleviate this problem, another parameter (ω), the inertia weight coefficient is introduced to original equation resulting into new velocity Eq. (30) of PSO (Eberhart and Shi 1998; Shi and Eberhart 1998)

$$V_i^{k+1} = \omega^k \times V_i^k + c_1 \times \text{rand}_1 \times (X_{\text{pbest}}^k - X_i^k)$$
$$+ c_2 \times \text{rand}_2 \times (X_{\text{sbest}}^k - X_i^k). \qquad (30)$$

The inertia weight (ω) can be assumed to follow a linearly decreasing pattern between maximum ($\omega_{\max}$) and minimum ($\omega_{\min}$) values as follows:

$$\omega^k = \omega_{\max} - (\omega_{\max} - \omega_{\min}) \frac{k}{k_{\max}}. \qquad (31)$$

Later, contemporary standard PSO (CS-PSO) version was developed by Clerc and Kennedy (2002) in which velocity of the particles is updated as follows:

$$V_i^{k+1} = \eta \times V_i^k + c_1 \times \text{rand}_1 \times (X_{\text{pbest}}^k - X_i^k)$$
$$+ c_2 \times \text{rand}_2 \times (X_{\text{sbest}}^k - X_i^k). \qquad (32)$$

For all the above cases-mentioned, particle's positions are updated as follows:

$$X_i^{k+1} = X_i^k + V_i^{k+1}. \qquad (33)$$

The constriction coefficient (η) is determined as suggested by Clerc and Kennedy (2002):

$$\eta = \frac{2}{\left| 2 - \phi - \sqrt{\phi^2 - 4\phi} \right|}, \qquad (34)$$

where $\phi = c_1 + c_2$.

The cognitive (c_1) and social (c_2) parameters in Eq. (34) in CS-PSO variant are considered equal to 2.05. In this present work, contemporary standard PSO with velocity clamping is used. This is required so that the modified velocity does not make the particle jump out from the domain of interest. A bound is applied as follows:

$$\left| V_i^{k+1} \right| \le V_{\max} \quad i = 1, 2, 3, 4, \dots, N. \qquad (35)$$

Restriction is also applied on the updated value of particle's position so that it will also not move beyond the search space A. A bound is applied as follows:

$$\left| X_i^{k+1} \right| \le X_{\max} \quad i = 1, 2, 3, 4, \dots, N. \qquad (36)$$

The upper and lower bound of particle position are expressed as $X_{\max} = \left(x_1^{\text{ub}}, x_{\text{r}}^{\text{ub}}, \alpha_1^{\text{ub}}, \alpha_{\text{r}}^{\text{ub}} \right)$ and $X_{\min} = \left(x_1^{\text{lb}}, x_{\text{r}}^{\text{lb}}, \alpha_1^{\text{lb}}, \alpha_{\text{r}}^{\text{lb}} \right)$, respectively.

Formulation of stability chart

Stability charts present a series of graphs which are useful for estimation of the factor of safety (FOS) of any slope with known geometry and material properties. These graphs eliminate the need for carrying out actual stability analysis of the slope and provide an alternative way for quick and efficient analysis of any slope. Ever since Taylor (1937) introduced stability charts for clayey slopes, many researchers embraced the idea to develop stability charts for rock slopes (Michalowski 2002, 2010; Gao et al. 2013; Eid 2014; Sun et al. 2017). The effects of the seismic loadings (Yang et al. 2004; Yang 2007) and pore pressure (Yang and Zou 2006) on the rock slope stability were considered. Li et al. (2008) suggested stability chart-based solution based on Hoek–Brown criteria using numerical limit analysis. Li et al. (2009) also proposed stability chart solution based on limit analysis methods consider with seismic effect for rock mass. In this analysis, Li et al. (2009) had adopted Pseudo-static method for determining the rock slope stability.

It is desirable to build such charts for rock slopes based on generalized Hoek–Brown strength criterion of rock mass (Hoek et al. 2002). In the present study, stability charts for rock slopes have been developed incorporating generalized Hoek–Brown material parameters. The FOS of the slope is determined using limit equilibrium method based Morgenstern and Price (1965) formulation. Particle Swarm Optimization (PSO) technique is used to determine the critical failure surface with global minimum FOS for rock slope stability problems. The associated material properties of rock mass are: uniaxial compressive strength (σ_{ci}), Geological Strength Index (GSI), intact rock mass parameter m_i, unit weight of rock mass (γ), height of slope (H) and slope angle (β). In this article, stability charts have been prepared for slope angles (β) = 15°, 30°, 45°, 60° and 75°. Considering a FOS F for any slope, the stability number is defined as:

$$N = \frac{\sigma_{ci}}{\gamma \mathrm{HF}}. \tag{37}$$

Results and discussion

In this paper, authors have strived to develop stability charts of rock slopes incorporating GHB criterion proposed by Hoek et al. (2002). Morgenstern and Price (1965) method based on limit equilibrium technique is adopted to determine the value of factor of safety of the rock slope against failure. An evolutionary optimization method i.e. Particle Swarm Optimization (PSO) is used to search for the minimum FOS values and the associated critical failure surface out of all possible slip surfaces. A MATLAB code has been developed for this purpose. The charts have been developed for entire range of Geological Strength Index (GSI) values ranging from 0 to 100 for intact rock mass characterized by the disturbance factor $D = 0$. The associated material properties of rock mass have been taken from the works of Li et al. (2008). The corresponding values of minimum FOS are presented in Table 1. The results presented in Table 1 show that minimum factor of safety (FOS) values decrease with increasing slope angle (β). It can also be observed that calculated stability numbers obtained from Eq. (37) decrease with increasing GSI and m_i.

Figure 3a–e present the rock stability charts for the rock slope angles $\beta = 15°$, $30°$, $45°$, $60°$ and $75°$ for range of GSI values and m_i mentioned in Table 1. The figures reveal that the stability numbers increase with increasing inclination angles of rock slope for given GSI and m_i. Correspondingly, factor of safety (FOS) will tend to decrease with increasing slope angle β. However, if any individual stability chart for any given slope angle is studied, it can be seen that the stability number N follows a decreasing pattern if the parameters GSI or m_i increase.

It is desirable to check the type of slope failure (i.e. base failure, face failure or toe failure) which will take place for the stability charts developed and presented in Fig. 3a–e. Figure 4a presents the critical failure surface (CFS) for the parameters GSI = 50, $m_i = 25$ and slope angle $\beta = 15^0$. It is seen that the induced slope failure corresponds to deep-seated base failure. For other values of material properties (i.e. GSI and m_i), base failures have been observed at the same slope angle (i.e. $\beta = 15°$). Figure 4b shows the CFS for the chosen rock parameters GSI = 50, $m_i = 25$ and $\beta = 30°$. However, in this case, toe failure is found to take place. Similarly, for $\beta = 45°$, $60°$ and $75°$, toe failures happen as observed in Fig. 4c–e, respectively. Furthermore, if the material parameters are altered for any give slope angle β (i.e. for either of $30°$, $45°$, $60°$ and $75°$), the observed

failure mode only corresponds to toe failure. Therefore, it may be inferred that base failure is the most likely mode failure for low value of slope angle β. If the slope angle increases (i.e. $\beta \geq 30°$), the mode of failure gradually shifts from base to toe failure. From this study, it is also observed that the value of factor of safety increases with decreasing slope angle of rock mass. For all the charts presented in Fig. 3a–e and CFS shown in Fig. 4a–e, Particle Swarm Optimization (PSO) method has been used to search the CFS. In the present study, the calculated values of stability numbers are very close to those obtained by Li et al. (2008, 2009) where limit analysis technique was used to perform slope analysis.

Stability charts for seismic loading conditions

Next, the stability charts have been developed for the rock slope considering the effect of seismic loading. During rock slope stability analysis, the intact rock mass has an uniaxial compressive strength (σ_{ci}), intact rock yield parameter (m_i), unit weight (γ) and geological strength index (GSI). These values are usually considered constant throughout the slope. The effect of seismic excitation is incorporated by considering the presence of an equivalent pseudo-static horizontal force equal to $k_h W$ acting on the slope mass. Here, k_h is the horizontal seismic coefficient and W is the weight of any slice. The limit equilibrium-based Morgenstern–Price method has been utilized to calculate the value of FOS of the rock slope. PSO is used to search for the CFS out of all considered failure surfaces along with the corresponding minimum FOS value of the slope.

In this study, the stability charts are developed considering for horizontal seismic coefficient $k_h = 0.1$, 0.15, 0.20, 0.25 and 0.30 with different slope angles $\beta = 15°$, $30°$, $45°$, $60°$ and $75°$, respectively. The stability charts shown in Fig. 5a–e correspond to the case $k_h = 0.1$ for different values of slope angle. If the stability charts are compared with those presented in Fig. 3a–e for non-seismic case, it is observed that the stability number N increases. Correspondingly, the FOS values for seismic case decrease compared to the non-seismic case. The stability charts presented in Fig. 5a–e follow similar trends with those presented for non-seismic case with respect to change in material parameters (i.e. GSI and m_i) and slope angle β. The stability number N follows a decreasing pattern with increasing values of GSI and m_i. On the other hand, if the slope angle β increases, the stability number N is found to increase with corresponding decrease in FOS value of the slope.

The stability charts shown in Fig. 6a–e correspond to the case when $k_h = 0.15$ for different values of slope angles. If

Table 1 Analysis of rock slope stability and develop the stability chart based on limit equilibrium M–P method (material properties as per Li et al. 2008)

Slope angle (β)	Geological Strength Index (GSI)	Hoek–Brown yield parameter (m_i)	$\sigma_{ci}/\gamma H$	FOS values from non-linear GHB criterion	Stability number (N) $N = \sigma_{ci}/\gamma HF$
15	100	5	0.026	1.280	0.0203
15	100	15	0.009	1.297	0.0069
15	100	25	0.005	1.252	0.0039
15	100	35	0.004	1.318	0.0030
15	70	5	0.078	1.296	0.0601
15	70	15	0.026	1.298	0.0200
15	70	25	0.015	1.277	0.0117
15	70	35	0.011	1.293	0.0085
15	50	5	0.158	1.295	0.1220
15	50	15	0.052	1.302	0.0399
15	50	25	0.031	1.305	0.0237
15	50	35	0.022	1.306	0.0168
15	30	5	0.334	1.301	0.2566
15	30	15	0.101	1.304	0.0774
15	30	25	0.058	1.306	0.0443
15	30	35	0.040	1.304	0.0306
15	10	5	0.994	1.325	0.7496
15	10	15	0.211	1.326	0.1591
15	10	25	0.103	1.328	0.0775
15	10	35	0.064	1.327	0.0482
30	100	5	0.070	1.005	0.0696
30	100	15	0.026	1.020	0.0254
30	100	25	0.016	1.027	0.0155
30	100	35	0.011	1.011	0.0108
30	70	5	0.218	1.010	0.2157
30	70	15	0.075	1.015	0.0738
30	70	25	0.045	1.015	0.0443
30	70	35	0.032	1.014	0.0315
30	50	5	0.461	1.013	0.4549
30	50	15	0.153	1.016	0.1504
30	50	25	0.091	1.017	0.0894
30	50	35	0.065	1.020	0.0636
30	30	15	0.323	1.018	0.3170
30	30	25	0.185	1.019	0.1815
30	30	35	0.129	1.021	0.1262
30	10	5	4.363	1.016	4.2909
30	10	15	0.943	1.020	0.9245
30	10	25	0.460	1.020	0.4506
30	10	35	0.286	1.020	0.2801
45	100	5	0.135	0.984	0.1371
45	100	15	0.058	0.996	0.0581
45	100	25	0.036	0.998	0.0360
45	100	35	0.026	0.998	0.0260
45	70	5	0.469	0.990	0.4734
45	70	15	0.176	0.999	0.1760
45	70	25	0.108	1.005	0.1074
45	70	35	0.077	1.004	0.0766
45	50	5	1.046	0.993	1.0529
45	50	15	0.369	1.003	0.3678
45	50	25	0.222	1.006	0.2205
45	50	35	0.158	1.007	0.1568

Table 1 (continued)

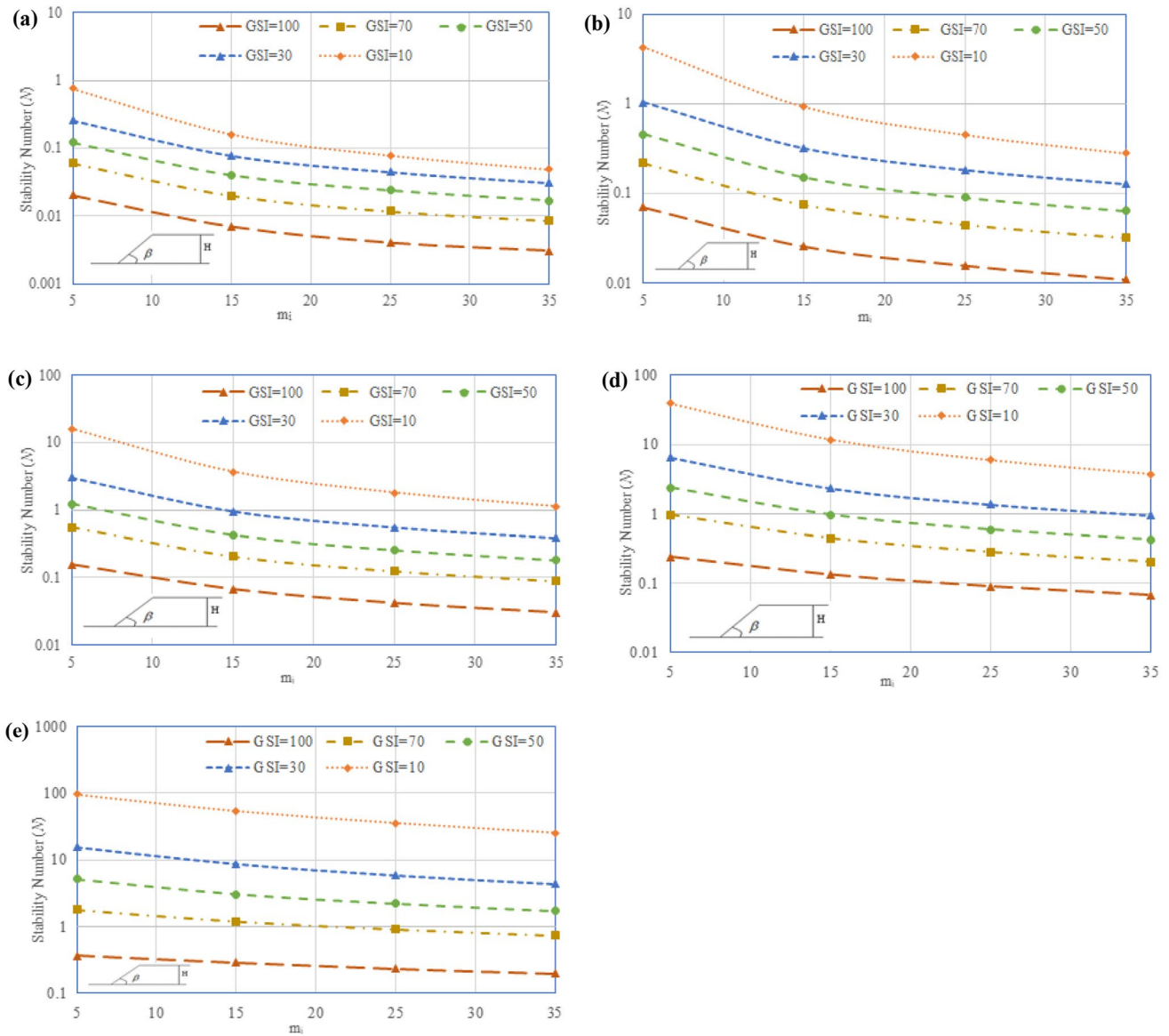| Slope angle (β)	Geological Strength Index (GSI)	Hoek–Brown yield parameter (m_i)	$\sigma_{ci}/\gamma H$	FOS values from non-linear GHB criterion	Stability number (N) $N = \sigma_{ci}/\gamma HF$
45	30	5	2.593	0.997	2.6008
45	30	15	0.829	1.005	0.8242
45	30	25	0.480	1.008	0.4757
45	30	35	0.334	1.010	0.3305
45	10	5	13.585	0.999	13.5918
45	10	15	3.155	1.007	3.1301
45	10	25	1.552	1.010	1.5364
45	10	35	0.969	1.010	0.9584
60	100	5	0.232	0.974	0.2379
60	100	15	0.130	0.987	0.1317
60	100	25	0.088	0.989	0.0889
60	100	35	0.066	0.991	0.0665
60	70	5	0.946	0.985	0.9604
60	70	15	0.435	0.989	0.4394
60	70	25	0.276	0.992	0.2781
60	70	35	0.200	0.992	0.2015
60	50	5	2.337	0.987	2.3662
60	50	15	0.953	0.991	0.9610
60	50	25	0.584	0.993	0.5880
60	50	35	0.419	0.994	0.4213
60	30	5	6.439	0.989	6.5050
60	30	15	2.317	0.994	2.3306
60	30	25	1.356	0.995	1.3619
60	30	35	0.945	0.996	0.9486
60	10	5	38.926	0.988	39.3879
60	10	15	11.734	0.998	11.7559
60	10	25	5.928	0.999	5.9308
60	10	35	3.729	1.0003	3.7277
75	100	5	0.36	0.986	0.3650
75	100	15	0.278	0.968	0.2870
75	100	25	0.228	0.976	0.2336
75	100	35	0.194	0.980	0.198
75	70	5	1.703	0.949	1.80
75	70	15	1.169	0.977	1.196
75	70	25	0.89	0.981	0.907
75	70	35	0.717	0.984	0.7280
75	50	5	4.98	0.972	5.120
75	50	15	2.988	0.980	3.046
75	50	25	2.156	0.985	2.187
75	50	35	1.668	0.987	1.688
75	30	5	15.011	0.970	15.467
75	30	15	8.576	0.984	8.7103
75	30	25	5.824	0.988	5.8923
75	30	35	4.327	0.990	4.369
75	10	5	93.721	0.970	96.523
75	10	15	53.362	0.986	54.082
75	10	25	35.186	0.991	35.489
75	10	35	24.994	0.993	25.155

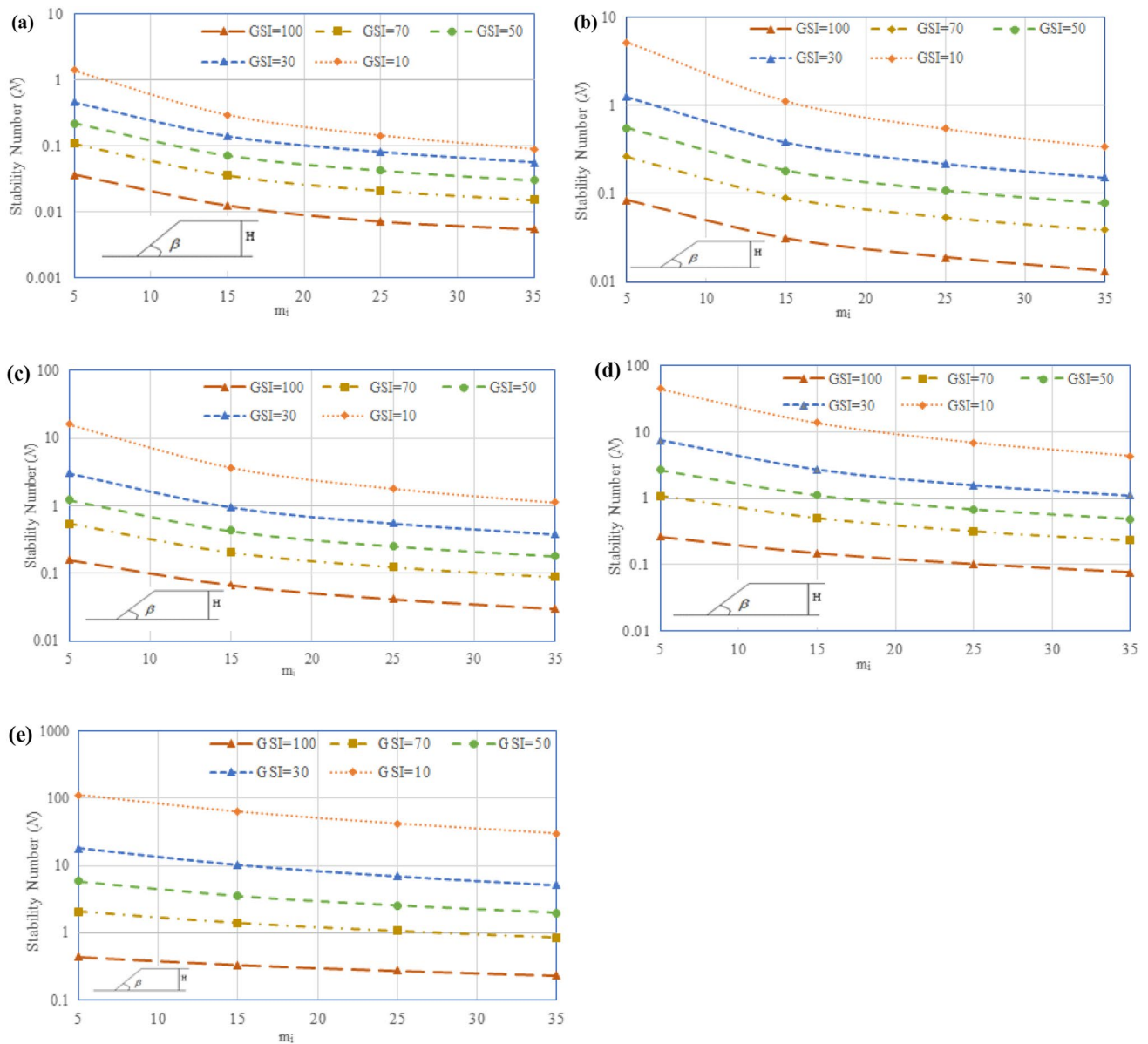**Fig. 3** Stability number from limit equilibrium M–P method at different GSI values for different slope angles **a** $\beta = 15°$, **b** $\beta = 30°$, **c** $\beta = 45°$, **d** $\beta = 60°$, **e** $\beta = 75°$

the stability charts are compared with those presented in Fig. 3a–e for non-seismic case and Fig. 5a–e for seismic case with $k_h = 0.10$, it is observed that the stability number N increases. Correspondingly, the FOS values for seismic case $k_h = 0.15$ decrease compared to the non-seismic case and for seismic case with $k_h = 0.10$.

The stability charts presented in Fig. 6a–e follow similar trends as those presented for non-seismic case and seismic

case for $k_h = 0.1$ with respect to change in material parameters (i.e. GSI and m_i) and slope angle β. The stability number N follows a decreasing trend with increasing values of GSI and m_i. On the other hand, if the slope angle β increases, the stability number N increases with corresponding decrease in FOS value of the slope.

Figure 7a–e show the stability charts with $k_h = 0.20$ for different values of slope angles $\beta = 15°$, 30°, 45°, 60° and
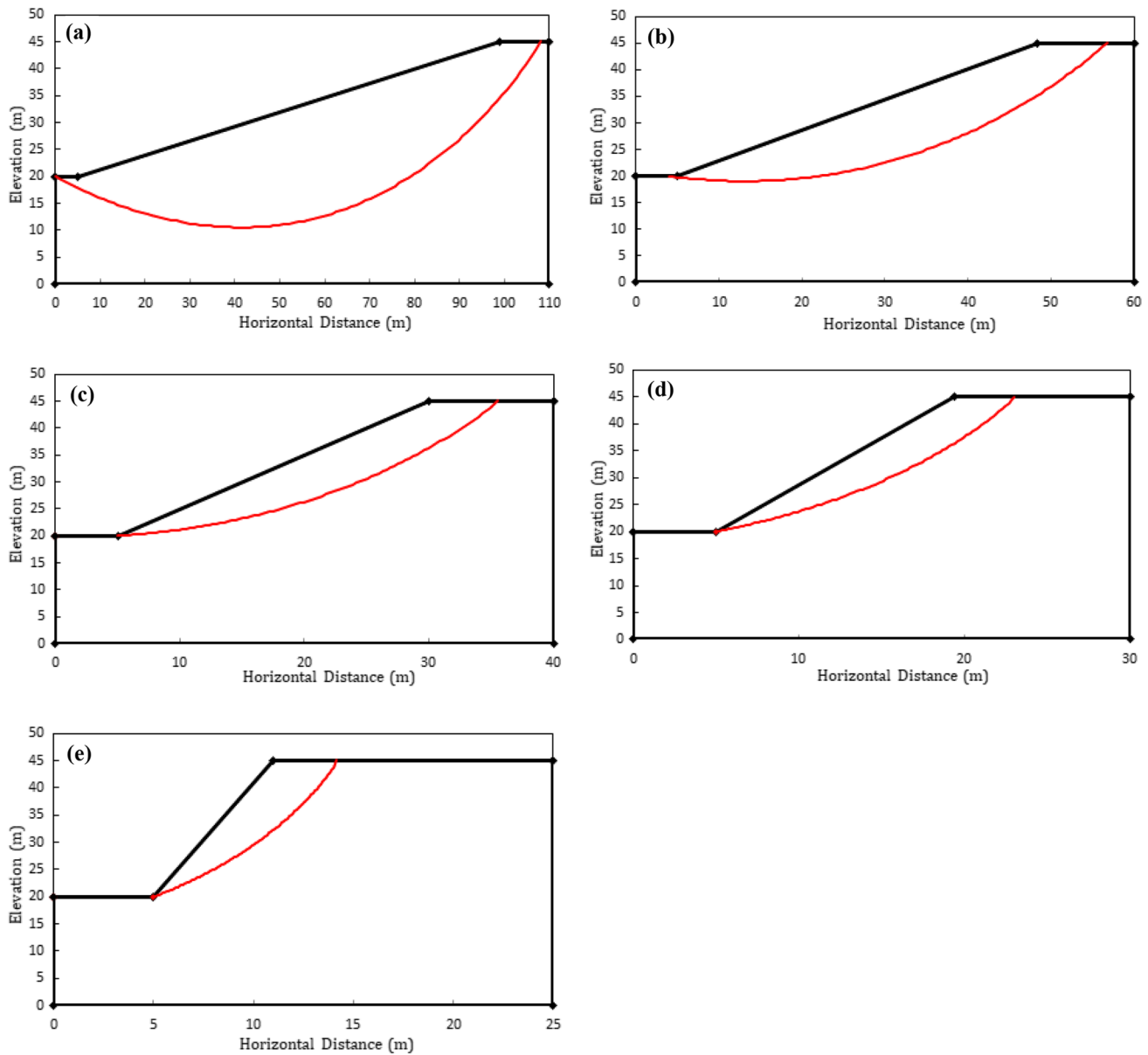
Fig. 4 Critical failure surface (CFS) for GSI = 50 and $m_{i} = 25$ at different slope angles **a** $\beta = 15°$, **b** $\beta = 30°$, **c** $\beta = 45°$, **d** $\beta = 60°$, **e** $\beta = 75°$

75°, respectively. In all these cases, the stability number N is found to increase with corresponding decrease in FOS values as the slope angle β and the horizontal seismic coefficient k_h increase. The nature of the stability charts is found to follow similar pattern with respect to change in material parameters i.e. GSI and m_i. If the values GSI and m_i increase signifying better-quality rocks, the stability

number N decreases with corresponding increase in FOS values.

In a similar manner, stability charts have been developed considering the value of horizontal seismic coefficient $k_h = 0.25$ which have been presented in Fig. 8a–e. If the stability charts for $k_h = 0.25$ are compared with previous cases, it can be seen that the stability number
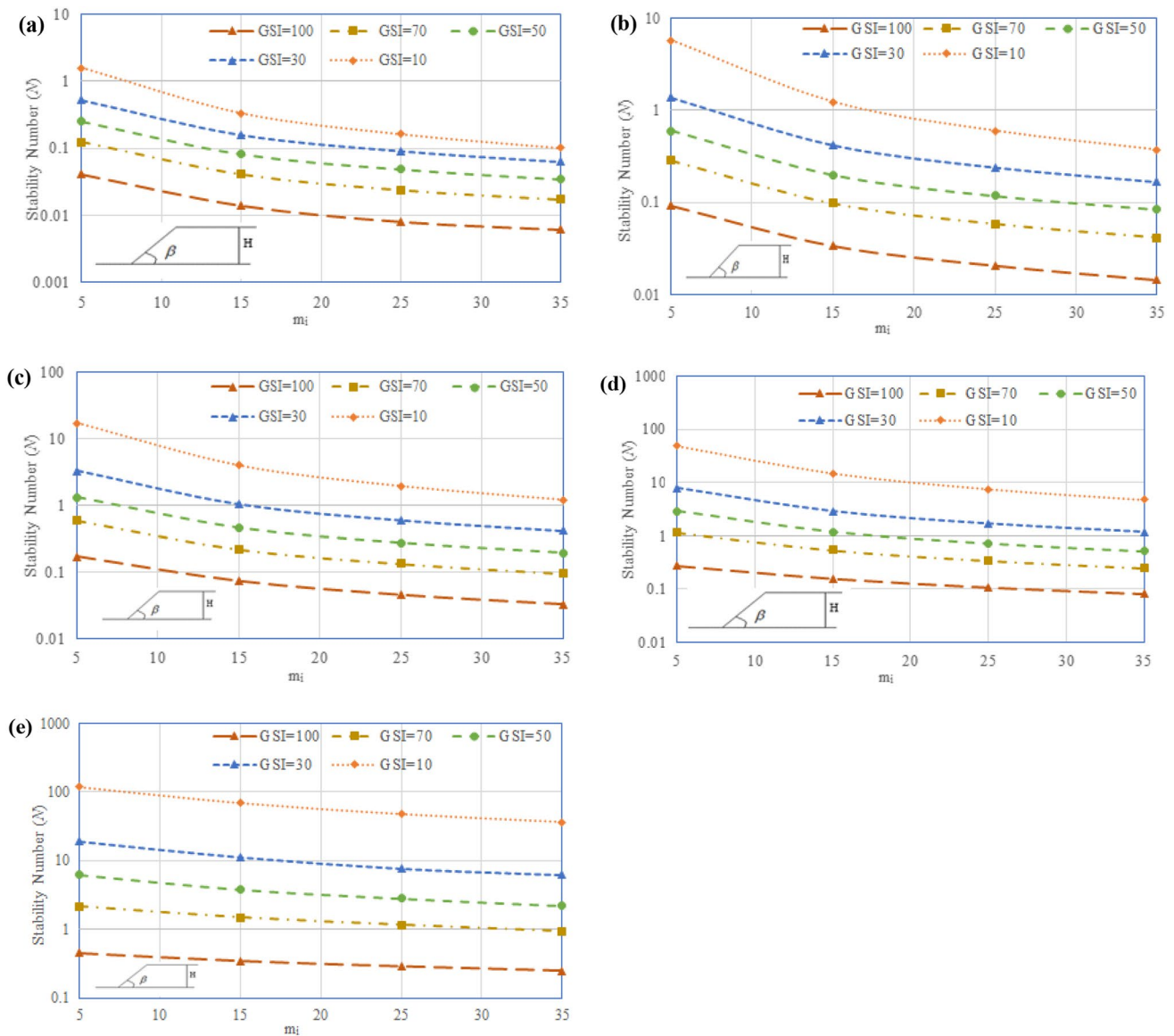
Fig. 5 Stability number from limit equilibrium M–P method at different GSI values with $k_h = 0.10$ for different slope angles **a** $\beta = 15°$, **b** $\beta = 30°$, **c** $\beta = 45°$, **d** $\beta = 60°$, **e** $\beta = 75°$

shifts upwards indicating corresponding fall in the value of factor of safety of the slope. However, the trends of Fig. 8a–e resemble the charts developed for lower values of k_h.

Also, stability charts have been developed for $k_h = 0.30$ for slope geometries with varying slope angles. These charts are presented in Fig. 9a–e. The nature of the stability charts again follows similar trend as previously discussed up to angle $\beta = 15°$, 30°, 45° and 60° in Fig. 9a–d. But the nature of the stability chart for angle $\beta = 75°$ and $k_h = 0.30$ has been found to be different in Fig. 9e. It is found that for $m_i \geq 15$ and GSI ≤ 50, the trend of variation of stability number becomes flatter with increase in m_i. Similar trends were reported by Li et al. (2009) for slope angle $\beta = 75°$ and $k_h = 0.30$. Generally, it is expected that FOS values should increase with corresponding improvement of material
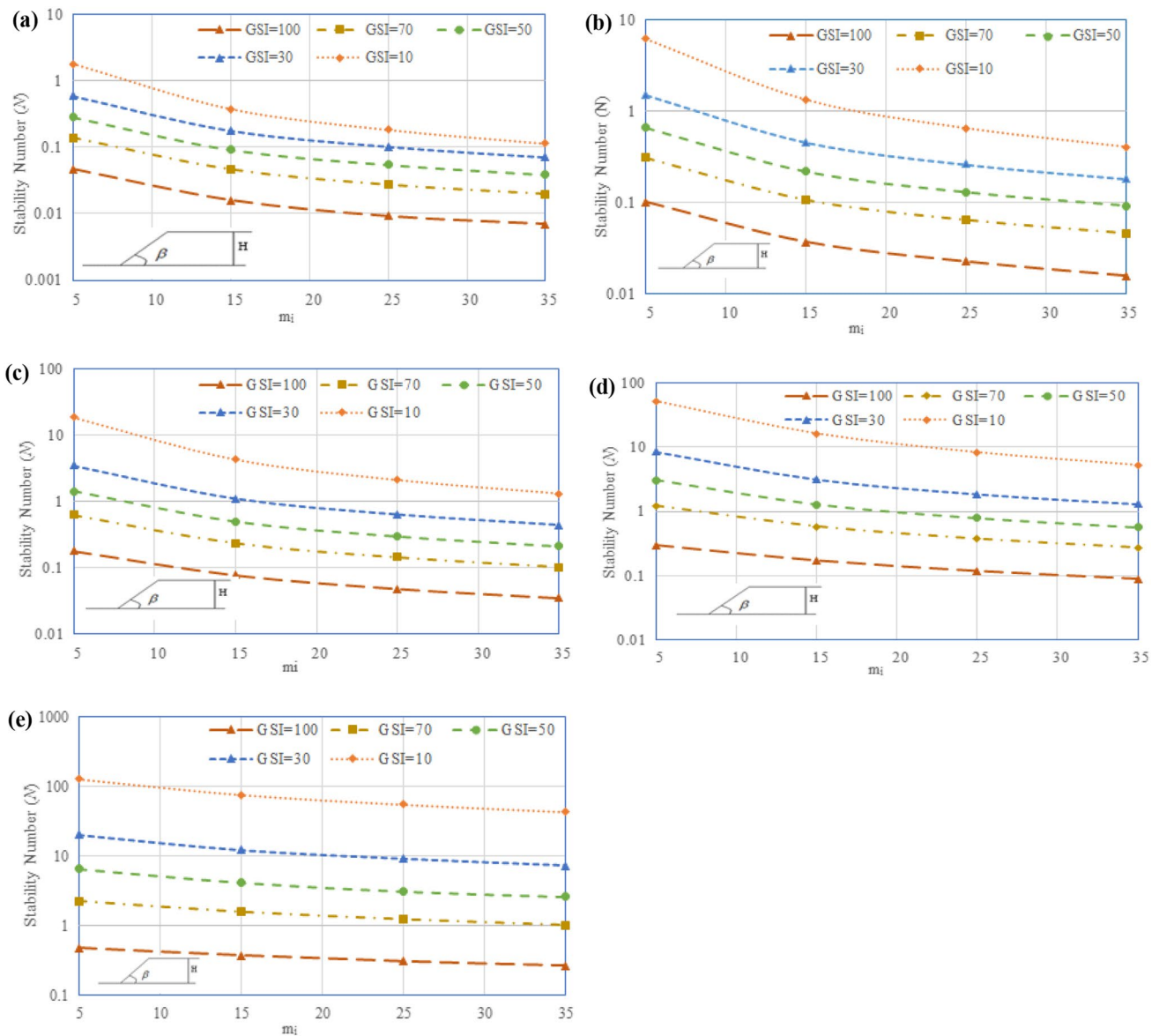
Fig. 6 Stability number from limit equilibrium M–P method at different GSI values with $k_h = 0.15$ for different slope angles **a** $\beta = 15°$, **b** $\beta = 30°$, **c** $\beta = 45°$, **d** $\beta = 60°$, **e** $\beta = 75°$

parameter m_i signifying better rock quality, a trend that did not emerge from Fig. 9e. Therefore, the results shown in Fig. 9e (for $\beta = 75°$ and $k_h = 0.30$) should be considered with caution. Hence, further investigations are necessary when rock slopes are analyzed for high slope angles and high lateral seismic coefficients considering Hoek–Brown strength criterion.

It would be interesting to investigate the nature of variation of stability number N with material parameter m_i

with changing values of horizontal seismic coefficients k_h. The other material parameter (i.e. GSI) is considered to be constant while developing the plots shown in Fig. 10a–e for different slope angles $\beta = 15°$, 30°, 45°, 60° and 75°, respectively. From Fig. 10a–e, it is observed that the stability number (N) of rock mass increases as the k_h value increases. Therefore, the FOS values of the slope will decrease correspondingly.

Fig. 7 Stability number from limit equilibrium M–P method at different GSI values with $k_h = 0.20$ for different slope angles **a** $\beta = 15°$, **b** $\beta = 30°$, **c** $\beta = 45°$, **d** $\beta = 60°$, **e** $\beta = 75°$

The variation between normalized major principal stresses $\left(\frac{\sigma_3}{\sigma_{ci}}\right)$ and minor principal stresses $\left(\frac{\sigma_1}{\sigma_{ci}}\right)$ has been calculated using Eq. (1) and presented in Fig. 11 for seismic loading case with ($k_h = 0.10$ and 0.30) for the entire extent of the failure surface. The material parameters considered are Geological strength index (GSI) = 100, $m_i = 15$ and 35 and slope angle (β) = 60°. It is observed that the range of principal stress values of intact rock mass at GSI = 100, $m_i = 35$ and $k_h = 0.10$ fall more in compression zone compared to GSI = 100, $m_i = 35$ and $k_h = 0.30$. Similar behavior is observed for intact rock mass with GSI = 100, $m_i = 15$ with $k_h = 0.10$ and 0.30. But the portion of principal stress is found to extend more towards tensile region when k_h is increased from 0.10 to 0.30. It is also found that the range of principal stress in the tension region is more for rock mass with GSI = 100 and $m_i = 15$ than GSI = 100 and $m_i = 35$.
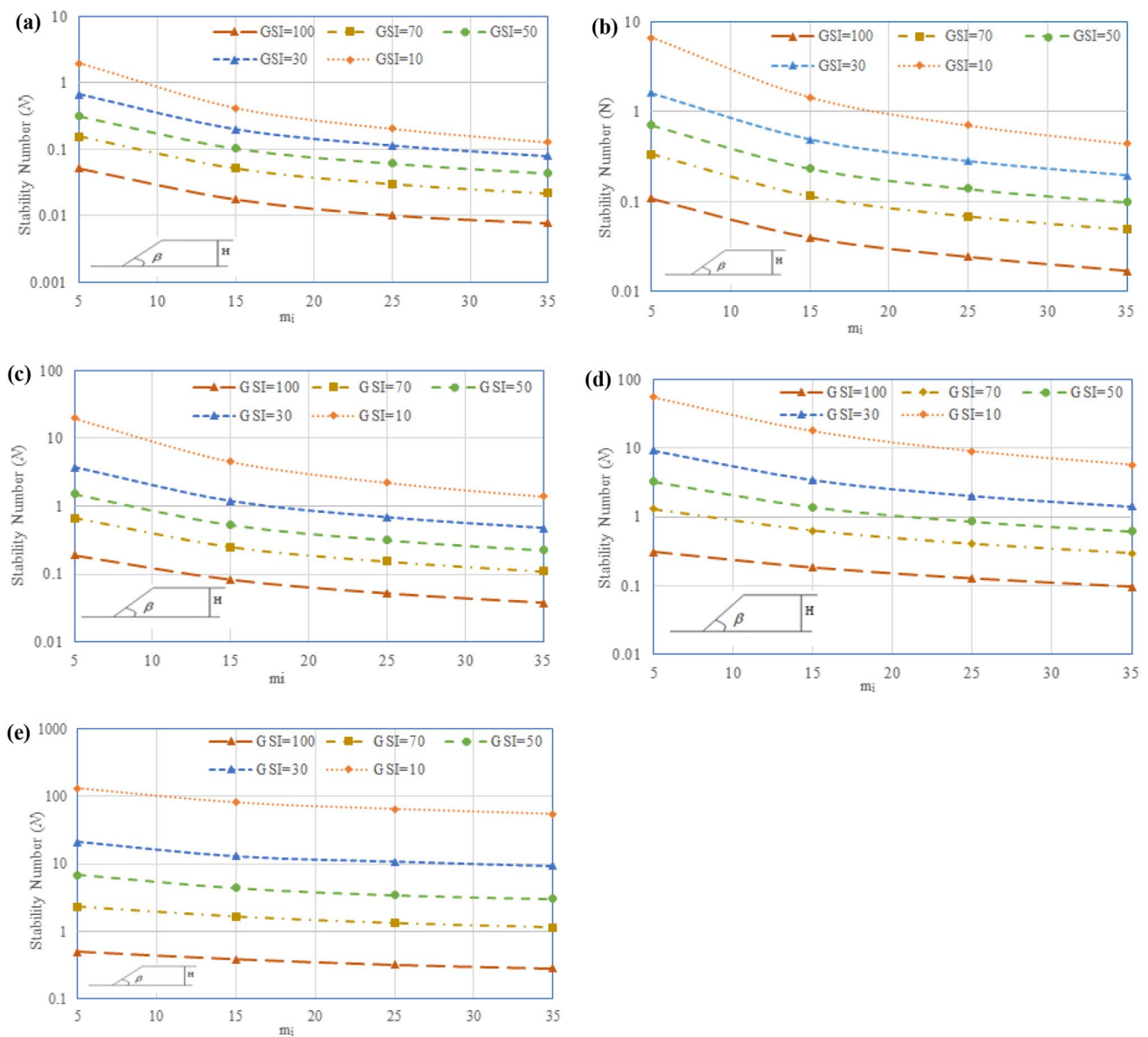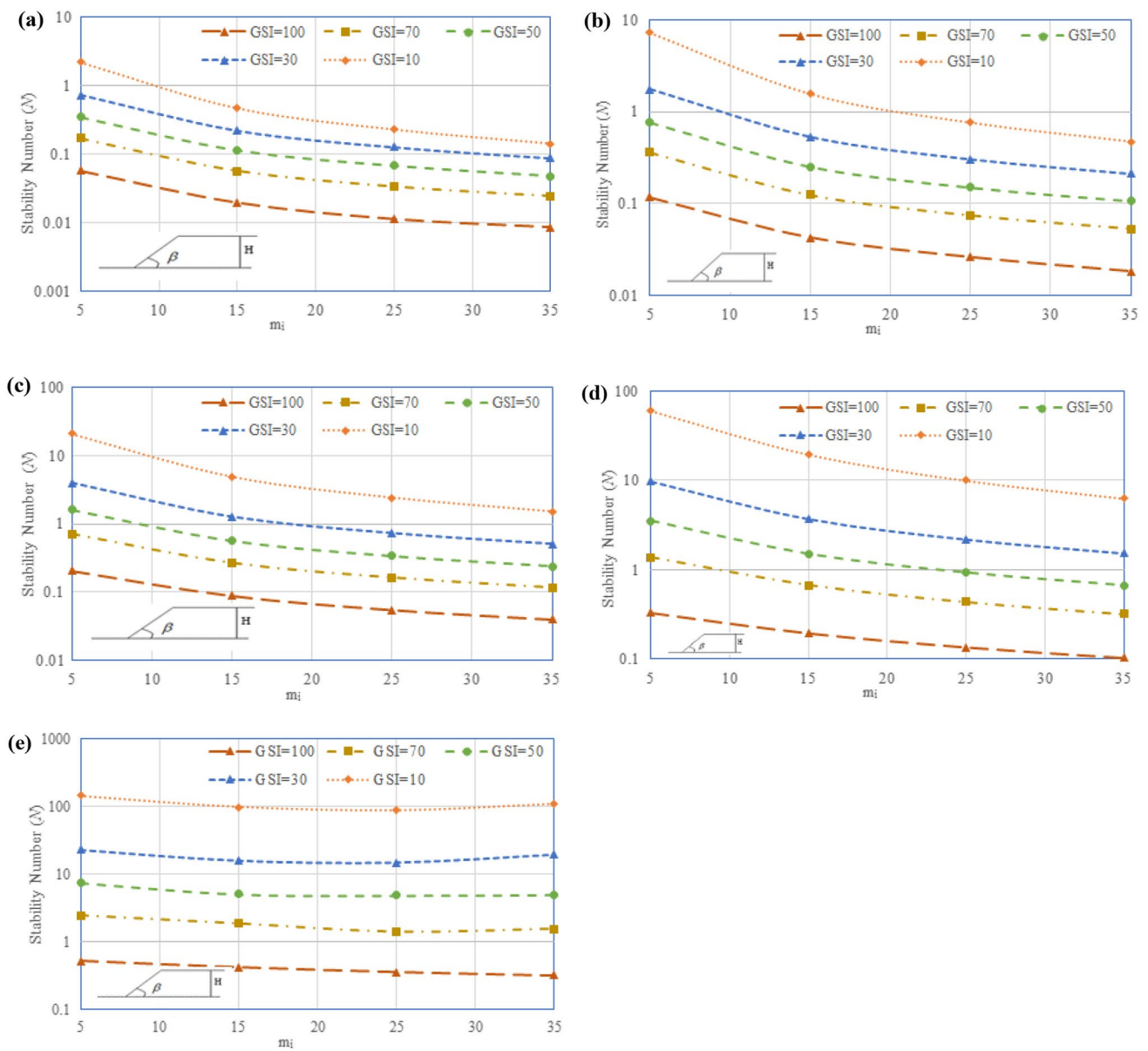
Fig. 8 Stability number from limit equilibrium M–P method at different GSI values with $k_h = 0.25$ for different slope angles (a) $\beta = 15^0$, (b) $\beta = 30^0$, (c) $\beta = 45^0$, (d) $\beta = 60^0$, (e) $\beta = 75^0$

Conclusions

In the present work, rock slope stability charts have been developed after incorporating the generalized Hoek–Brown strength criterion suggested by Hoek et al.(2002). Morgenstern and Price (1965) method has been used to determine the FOS of the rock slopes with failure surfaces assumed to be composed of piecewise linear segments.

An evolutionary optimization method i.e. Contemporary Standard Particle swarm optimization (CS-PSO) has been used to search for the minimum FOS values and the associated critical failure surface. The charts have been developed for entire range of Geological Strength Index (GSI) values ranging from 0 to 100 for intact rock mass characterized by the disturbance factor $D = 0$. It is observed that the stability numbers follow an increasing pattern as the

Fig. 9 Stability number from limit equilibrium M–P method at different GSI values with $k_h=0.30$ for different slope angles **a** $\beta = 15°$, **b** $\beta = 30°$, **c** $\beta = 45°$, **d** $\beta = 60°$, **e** $\beta = 75°$

slope inclination increases. Also, the stability numbers follow a decreasing trend as the Hoek–Brown material parameter m_i and GSI increase.

Both static and seismic analyses have been carried out while developing the stability charts for intact rock mass. The charts have been developed for slopes with inclination angles $\beta = 15°$, $30°$, $45°$, $60°$ and $75°$, respectively. When the slope angle is less (i.e. $\beta \leq 15°$), the mode of failure

is identified as base failure. The mode of failure gradually shifts towards toe failure as the slope angle increases. Five values of horizontal seismic coefficient i.e. 0.10, 0.15, 0.20, 0.25 and 0.30 have been used while developing the stability charts for seismic loading condition. As the slope inclination increase, the stability numbers increase with corresponding reduction in associated factor of safety for both static and seismic case. Furthermore, it is also
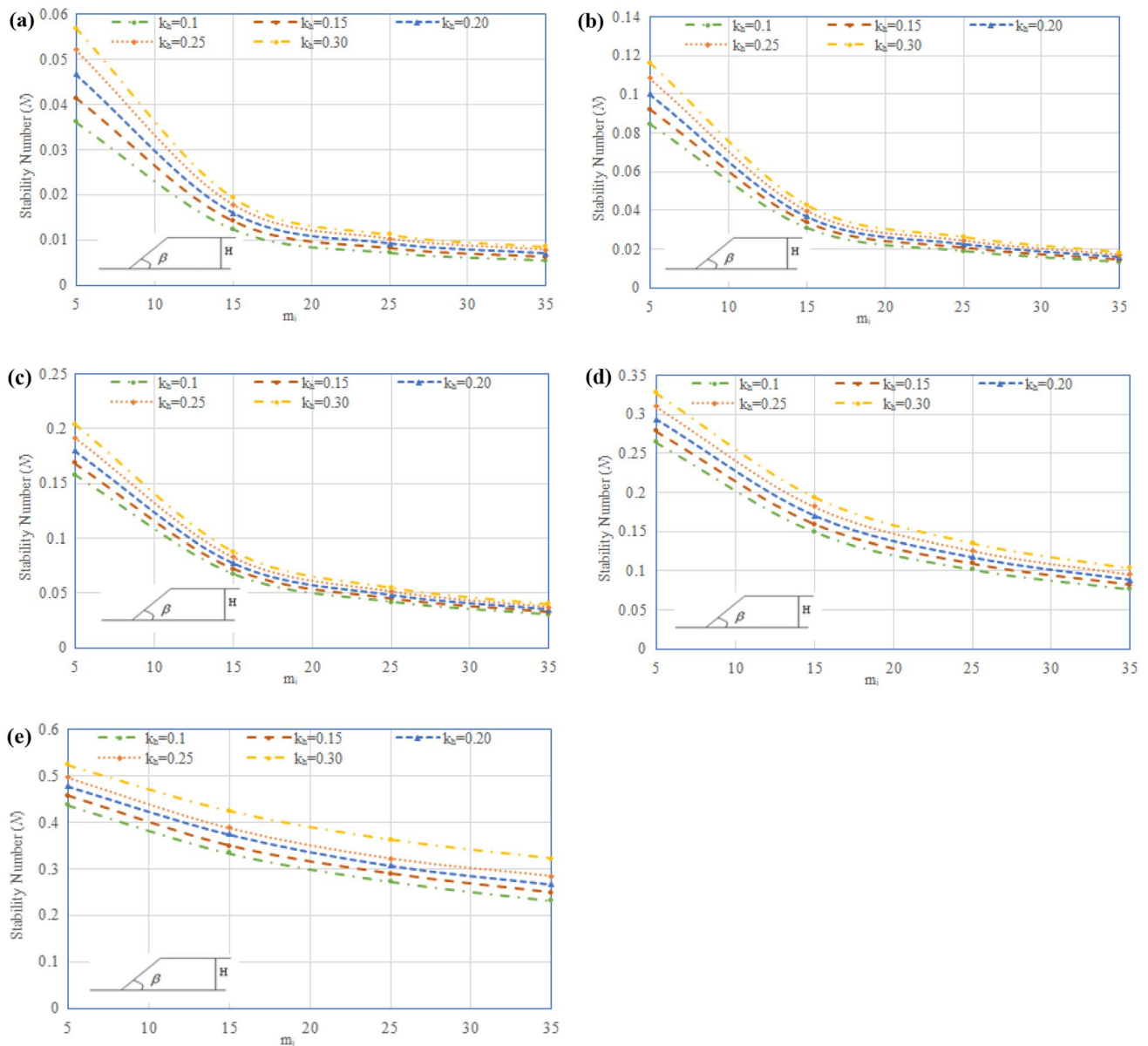
Fig. 10 Stability number for different horizontal seismic coefficient (k_h) at different slope angles **a** $\beta = 15°$, **b** $\beta = 30°$, **c** $\beta = 45°$, **d** $\beta = 60°$, **e** $\beta = 75°$

observed that the stability of the slope is adversely affected when higher seismic loading is applied. These results into increase in stability numbers compared to non-seismic case. It is observed that the nature of stability charts become flattish for high angle of inclination ($\beta \geq 75°$) and horizontal seismic coefficient $k_h \geq 0.30$ with increasing m_i values, a trend which does not quite fit with general notion. A decreasing trend of stability number N with improving m_i values would have more in the line with expectation.

Therefore, this particular aspect deserves further attention from the researchers.

If the nature of principal stresses along the failure surface is observed, it can be found that the stresses increasingly shift towards tensile region as the magnitude of seismic loading and the slope inclination are increased. On the other hand, if the Hoek–Brown material constants i.e. GSI and m_i values are increased, the pattern of principal stresses along the failure surface shift towards compression region.
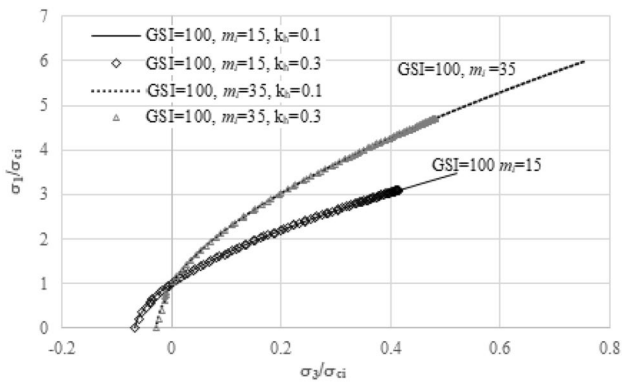
Fig. 11 The Hoek–Brown failure envelop for variable m_i and horizontal seismic coefficient (k_h) with $\beta = 60^0$

Compliance with ethical standards

Conflict of interest As per authors' knowledge, the present work has no conflict interest with any other work. No financial assistance was required for this work.

References

Balmer G (1952) A general analytical solution for Mohr's envelope. Am Soc Test Mat 52:1269–1271

Basahel H, Mitri H (2017) Application of rock mass classification systems to rock slope stability assessment: a case study. J Rock Mech Geotech Eng 9(6):993–1009. https://doi.org/10.1016/j.jrmge.2017.07.007

Belghali M, Saada Z, Garnier D, Maghous S (2017) Pseudo-static stability analysis of rock slopes reinforced by passive bolts using the generalized Hoek–Brown criterion. J Rock Mech Geotech Eng 9(4):659–670. https://doi.org/10.1016/j.jrmge.2016.12.007

Bishop AW (1955) The use of the slip circle in the stability analysis of slopes. Géotechnique 5:7–17. https://doi.org/10.1680/geot.1955.5.1.7

Carranza-Torres C (2004) Elasto-plastic solution of tunnel problems using the generalized form of the Hoek–Brown failure criterion. Int J Rock Mech Min Sci 41:629–639. https://doi.org/10.1016/j.ijrmms.2004.03.111

Cheng YM, Li L, Chi SC, Wei WB (2007a) Particle swarm optimization algorithm for the location of the critical non-circular failure surface in twodimensional slope stability analysis. Comput Geotech 34(2):92–103

Cheng YM, Li L, Chi SC, Wei WB (2007b) Performance studies on six heuristic global optimization methods in the location of critical slip surface. Comput Geotech 34(6):462–484

Clerc M, Kennedy J (2002) The particle swarm—explosion, stability, and convergence in a multidimensional complex space. IEEE Trans Evol Comput 6:58–73. https://doi.org/10.1109/4235.985692

Deng D, Zhao L, Li L (2017) Limit equilibrium analysis for rock slope stability using basic Hoek–Brown strength criterion. J Cent South Univ 24:2154–2163. https://doi.org/10.1007/s11771-017-3624-4

Eberhart R, Kennedy J (1995) A new optimizer using particle swarm theory. In: Proceedings of 6th symposium on micro machine and human science. Nagoya, Japan, pp 39–43

Eberhart RC, Shi Y (1998) Comparison between genetic algorithms and particle swarm optimization. In: Lecture notes in computer science (including subseries lecture notes in artificial intelligence and lecture notes in bioinformatics). Berlin, pp 611–616

Eberhart R, Simpson P, Dobbins R (1996) Computational intelligence PC tools. Academic Press, New York

Eid HT (2014) Stability charts for uniform slopes in soils with nonlinear failure envelopes. Eng Geol 168:38–45

Fellenius W (1936) Calculation of stability of earth dams. Proc Second Congr Large Dams 4:445–463

Gao Y, Zhang F, Lei GH, Li D, Wu Y, Zhang N (2013) Stability charts for 3D failures of homogeneous slopes. J Geotech Geoenviron Eng 139(9):1528–1538

Goodman R (1989) Introduction to rock mechanics, 2nd edn. Wiley, New York

Goodman R, Kieffer D (2000) Behavior of rock in slope. J Geotech Geoenviron Eng 126:675–684

Himanshu N, Burman A, Kumar V (2019) Assessment of optimum location of non-circular failure surface in soil slope using unified Particle Swarm Optimization. Geotech Geol Eng. 38:2061–2083. https://doi.org/10.1007/s10706-019-01148-w

Himanshu N, Kumar V, Burman A, Gordan B (2020) Optimization of non-circular failure surface in slope based on particle swarm models. Innov Infrastruct Solut 5:9. https://doi.org/10.1007/s41062-019-0259-3

Hoek E (1983) Strength of jointed rock masses. Geotechnique 33:187–223

Hoek E, Bray J (1981) Rock slope engineering, 3rd edn. Institute of Mining and Metallurgy, London

Hoek E, Brown E (1980) Empirical strength criterion for rock masses. J Geotech Eng Div Am Soc Civ Eng 106(GT9):1013–1035

Hoek E, Brown ET (1997) Practical estimates of rock mass strength. Int J Rock Mech Min Sci 34:1165–1186. https://doi.org/10.1016/S1365-1609(97)80069-X

Hoek E, Brown ET (2019) The Hoek–Brown failure criterion and GSI—2018 edition. J Rock Mech Geotech Eng 11(3):445–463. https://doi.org/10.1016/j.jrmge.2018.08.001

Hoek E, Carranza-Torres C, Corkum B (2002) Hoek–Brown criterion—2002 edition. In: NARMS-TAC Conference, Toronto

Huang J, Lyamin AV, Griffiths DV, Krabbenhoft K, Sloan SW (2013) Quantitative risk assessment of landslide by limit analyses and random fields. Comput Geotech 53:60–67

Ismael MA, Imam HF, El-Shayeb Y (2014) A simplified approach to directly consider intact rock anisotropy in Hoek–Brown failure criterion. J Rock Mech Geotech Eng 6(5):486–492. https://doi.org/10.1016/j.jrmge.2014.06.003

Jaeger J (1971) Friction of rocks and stability of rock slopes. Geotechnique 21:97–134

Janbu N (1954) Applications of composite slip surfaces for stability analyses. Proc Eur Conf Stab Earth Slopes Stock 3:39–43

Kennedy J, Eberhart R (1995) Particle swarm optimization. In: Proceedings of the IEEE international conference on neural networks, Perth, Australia, pp 1942–1948

Krabbenhoft K, Lyamin AV, Hjiaj M, Sloan SW (2005) A new discontinuous upper bound limit analysis formulation. Int J Numer Methods Eng 63:1069–1088. https://doi.org/10.1002/nme.1314

Kumar P (1998) Shear failure envelope of Hoek–Brown criterion for rockmass. Tunn Undergr Space Technol 13(4):453–458. https://doi.org/10.1016/S0886-7798(98)00088-1

Kumar V, Burman A, Himanshu N, Barman B (2019a) Solution of minor principal stress for generalized Hoek–Brown rock material in two dimension using Newton–Raphson method. Geotech Geol Eng 38:1817–1837. https://doi.org/10.1007/s10706-019-01132-4

Kumar V, Himanshu N, Burman A (2019b) Rock slope analysis with nonlinear Hoek–Brown criterion incorporating equivalent Mohr–Coulomb parameters. Geotech Geol Eng 37:4741–4757. https://doi.org/10.1007/s10706-019-00935-9

Li AJ, Merifield RS, Lyamin AV (2008) Stability charts for rock slopes based on the Hoek–Brown failure criterion. Int J Rock Mech Min Sci 45:689–700. https://doi.org/10.1016/j.ijrmms.2007.08.010

Li AJ, Lyamin AV, Merifield RS (2009) Seismic rock slope stability charts based on limit analysis methods. Comput Geotech 36:135–148. https://doi.org/10.1016/j.compgeo.2008.01.004

Londe P (1988) Discussion of "Determination of the shear failure envelope in rock masses" by Roberto Ucar (March, 1986, Vol. 112, No. 3). J Geotech Eng 114:374–376. https://doi.org/10.1061/(ASCE)0733-9410(1988)114:3(374)

Lowe L, Karafiath L (1960) Stability of earth dams upon drawdown. In: Proceedings of the first PanAmerican conference on soil mechanics and fundation engineering

Lyamin A, Sloan S (2002) Lower bound limit analysis using non-linear programming. Int J Numer Methods Eng 55:573–611

Malkawi AIH, Hassan WF, Sarma SK (2001) Global search method for locating general slip surface Using Monte Carlo techniques. J Geotech Geoenviron Eng 127(8):688–698

McCombie P, Wilkinson P (2002) The use of the simple genetic algorithm in finding the critical factor of safety in slope stability analysis. Comput Geotech 29(8):699–714

Michalowski RL (2002) Stability charts for uniform slopes. J Geotech Geoenviron Eng 128(4):351–355

Michalowski RL (2010) Limit analysis and stability charts for 3D slope failures. J Geotech Geoenviron Eng 136(4):583–593

Morgenstern NR, Price VE (1965) The analysis of the stability of general slip surfaces. Géotechnique 15:79–93. https://doi.org/10.1680/geot.1965.15.1.79

Priest SD (2005) Determination of shear strength and three-dimensional yield strength for the Hoek–Brown criterion. Rock Mech Rock Eng 38(4):299–327. https://doi.org/10.1007/s00603-005-0056-5

Sari M (2019) Stability analysis of cut slopes using empirical, kinematical, numerical and limit equilibrium methods: case of old Jeddah-Mecca road (Saudi Arabia). Environ Earth Sci 78:621. https://doi.org/10.1007/s12665-019-8573-9

Shen J, Priest SD, Karakus M (2012b) Determination of Mohr–Coulomb shear strength parameters from generalized Hoek–Brown criterion for slope stability analysis. Rock Mech Rock Eng 45:123–129. https://doi.org/10.1007/s00603-011-0184-z

Shen J, Karakus M, Xu C (2012a) Direct expressions for linearization of shear strength envelopes given by the generalized Hoek–Brown criterion using genetic programming. Comput Geotech 44:139–146. https://doi.org/10.1016/j.compgeo.2012.04.008

Shi Y, Eberhart RC (1998) Parameter selection in particle swarm optimization. In: Lecture notes in computer science (including subseries lecture notes in artificial intelligence and lecture notes in bioinformatics). London 1447, pp 591–600

Shi Y, Eberhart RC (2008) Population diversity of particle swarms. In: 2008 IEEE congress on evolutionary computation, CEC 2008. pp 1063–1067

Shi X, Yang X, Meng Y, Li G (2016) Modified Hoek–Brown failure criterion for anisotropic rocks. Environ Earth Sci 75:995. https://doi.org/10.1007/s12665-016-5810-3

Siad L (2003) Seismic stability analysis of fractured rock slopes by yield design theory. Soil Dyn Earthq Eng 23:203–212

Spencer E (1967) A method of analysis of the stability of embankments assuming parallel inter-slice forces. Géotechnique 17:11–26. https://doi.org/10.1680/geot.1967.17.1.11

Sun C, Chai J, Xu Z, Qin Y (2017) 3D stability charts for convex and concave slopes in plan view with homogeneous soil based on the strength-reduction method. Intl J Geomech 17(5):06016034

Sun Z, Kong L, Guo A et al (2019) Experimental and numerical investigations of the seismic response of a rock–soil mixture deposit slope. Environ Earth Sci 78:716. https://doi.org/10.1007/s12665-019-8717-y

Taylor D (1937) Stability of earth slopes. J Bost Soc Civ Eng 24:197–246

Yang XL (2007) Seismic displacement of rock slopes with nonlinear Hoek-Brown failure criterion. Int J Rock Mech Mining Sci 44:948–953

Yang X-L, Li L, Yin J-H (2004) Seismic and static stability analysis for rock slopes by a kinematical approach. Géotechnique 54(8):543–549

Yang XL, Zou JF (2006) Stability factors for rock slopes subjected to pore water pressure based on the Hoek-Brown failure criterion. Int J Rock Mech Mining Sci 43:1146–1152

Wyllie D, Mah C (2004) Rock slope engineering, 4th edn. Spon Press, London

Zanbak C (1983) Design charts for rock slopes susceptible to toppling. J Geotech Eng Div ASCE 190:1039–1062

Zhu DY, Lee CF, Qian QH, Chen GR (2005) A concise algorithm for computing the factor of safety using the Morgenstern–Price method. Can Geotech J 42:272–278. https://doi.org/10.1139/t04-072

Zuo J, Liu H, Li H (2015) A theoretical derivation of the Hoek–Brown failure criterion for rock materials. J Rock Mech Geotech Eng 7(4):361–366. https://doi.org/10.1016/j.jrmge.2015.03.008